Inorganic Chemistry

Article

pubs.acs.org/IC

Unravelling the S → O Linkage Photoisomerization Mechanisms in *cis*- and *trans*-$[Ru(bpy)_2(DMSO)_2]^{2+}$ Using Density Functional Theory

Adrien J. Göttle, Fabienne Alary, Isabelle M. Dixon, Jean-Louis Heully, and Martial Boggio-Pasqua*

Laboratoire de Chimie et Physique Quantiques, UMR 5626 CNRS/Université Paul Sabatier-Toulouse III, 118 route de Narbonne, 31062 Toulouse, France

Supporting Information

ABSTRACT: A mechanistic study of the intramolecular S → O linkage photoisomerization in the cis and trans isomers of $[Ru(bpy)_2(DMSO)_2]^{2+}$ was performed using density functional theory. This study reveals that for the cis isomer the linkage photoisomerization of the two DMSO ligands occurs sequentially in the lowest triplet excited state and can either be achieved by a one-photon or by a two-photon mechanism. A mechanistic picture of the S → O photoisomerization of the trans isomer is also proposed. This work especially highlights that both adiabatic and nonadiabatic processes are involved in these mechanisms and that their coexistence is responsible for the rich photophysics and photochemical properties observed experimentally for the studied complexes. The different luminescent behavior experimentally observed at low temperature between the cis and trans isomers is rationalized based on the peculiarity of the topology of the triplet excited-state potential energy surfaces.

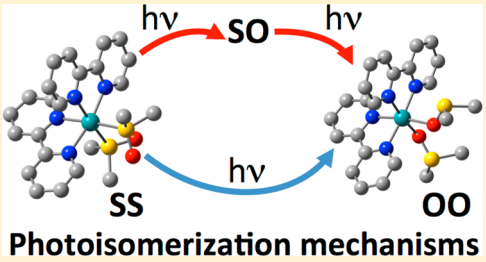

1. INTRODUCTION

Photoswitchable molecules and materials are compounds that display the capability to switch, under irradiation, between different isomers. Among these compounds, those which feature significantly different absorption properties following their photoswitching are said to be photochromic. Such compounds have been used in molecular computing[1−3] (logic gates), in photomechanical or opto-mechanical materials[4−8] and for biological applications.[9,10] Phototriggered linkage isomerization reactions are of particular interest for photochromism because they can imply drastic changes in the electronic structure and consequently, dramatic changes in the absorption properties.[11−16] In this latter case, there has been a growing interest over the past decade in designing photochromic polypyridyl sulfoxide ruthenium complexes[17−24] since the report of a phototriggered S → O linkage isomerization in *cis*-$[Ru(bpy)_2(DMSO)_2]^{2+}$ (where bpy = 2,2′-bipyridine and DMSO = dimethyl sulfoxide).[25] These complexes are particularly valuable for photochromism since they combine the well-known absorption properties of ruthenium polypyridyl complexes (low energy singlet metal-to-ligand charge transfer excitations) together with the linkage isomerization capability of the ambidentate sulfoxide ligands. The history and recent advances in this area have been recently reviewed.[26,27]

Theoretical studies of photochromic compounds aiming at describing the photoisomerization mechanism are largely limited to organic chromophores.[28−39] To our knowledge, the first study dealing with the excited state linkage isomerization mechanism of polypyridine ruthenium photochromic compounds dates back to 2003 and showed that DFT could be used to investigate such complex mechanisms.[40] In a more recent contribution, DFT calculations were performed to characterize the complete excited-state pathway for the S → O linkage isomerization in sulfoxide complexes. This study revealed that low lying triplet metal centered excited states (^{3}MC) play a crucial role in the intramolecular linkage photoisomerization of the bidentate OSO ligand (where OSO: 2-methylsulfinylbenzoate) in $[Ru(bpy)_2(OSO)]^+$.[41] Indeed, following the population of the lowest ^{3}MLCT state that already elongates the Ru−S bond, the antibonding character of MC states enables the large structural rearrangement occurring during the adiabatic isomerization on the lowest triplet excited-state potential energy surface (PES) and they also permit nonradiative deactivation of the complex toward the ground state (GS) by intersystem crossing[42] (ISC).[41] This result shed a new light on the photoisomerization mechanism, since some arguments against the implication of ^{3}MC states in the S → O linkage photoisomerization were proposed to rationalize several observations. First, differences in the evolution of the photoisomerization and photosubstitution quantum yields varying one of the ancillary ligands was argumented against the role of ^{3}MC states.[43,44] Second, the observation of S → O linkage photoisomerization in an osmium sulfoxide complex was used to rule out the role of ^{3}MC states, as these states are inaccessible in Os^{2+} complexes.[26,27,45] Moreover, calculations showed that ^{3}MC states were lying high in energy at the ground-state geometry in some ruthenium sulfoxide complexes.[46] Finally, following a femtosecond transient absorption spectroscopy study, ^{3}MLCT states were only invoked in the photoisomerization mechanism.[21] However, recent experimental contributions showed that multiple intermediates are formed

Received: March 10, 2014
Published: June 16, 2014

   dx.doi.org/10.1021/ic500546q | *Inorg. Chem.* 2014, 53, 6752−6760

sequentially on the lowest triplet PES and on a picosecond time scale after initial relaxation to the ^{3}MLCT state.[21,47,48] The implication of ^{3}MC states to enhance the Ru−S bond breaking occurring during the photoisomerization is now clearly raised.[47,48]

To further advance our theoretical investigation of photo-triggered linkage isomerization in ruthenium polypyridyl sulfoxide complexes, we were interested in studying the photochemistry of *cis*- and *trans*-$[Ru(bpy)_2(DMSO)_2]^{2+}$. These complexes are particularly interesting since a lot of data have been reported in two detailed experimental investigations.[18,25] The coordination scheme around the ruthenium of the cis and trans isomers is depicted in Scheme 1. For the cis isomer, both DMSO ligands are S-bonded (*cis*-SS) and for the trans isomer, one DMSO ligand is S-bonded and the other one is O-bonded (*trans*-SO). Irradiation of the *cis*-SS isomer leads to the S → O linkage isomerization of both DMSO ligands which results in the formation of a photoisomer with two O-bonded DMSO ligands (*cis*-OO) (Scheme 2). This metastable species reverts at room temperature and in the dark to the stable *cis*-SS state in a two-step process with the sequential O → S linkage isomerization of each DMSO ligand. During this process, an intermediate species is formed, in which one DMSO ligand is S-bonded and the other one is O-bonded (*cis*-SO). For the trans isomer, irradiation of the *trans*-SO complex yields the linkage isomerization of the S-bonded DMSO ligand and the formation the *trans*-OO isomer (Scheme 2). This metastable species reverts at room temperature and in the dark to the stable *trans*-SO state. Experimental data for the thermal back isomerization reactions have been reported[25] but the photoisomerization mechanism remains unclear. Nevertheless, Rack et al. reported some important information on the excited state behavior. The photochromism of $[Ru(bpy)_2(DMSO)_2]^{2+}$ is temperature dependent, with both cis and trans isomers displaying photochromic properties at room temperature but not at 77 K.[18] They also observed that the trans isomer was not emissive, whereas the cis isomer displayed low temperature emission from a doubly S-bonded structure (*cis*-SS).

Scheme 1. Coordination Scheme around the Ruthenium of the *cis*-SS and *trans*-SO Structures

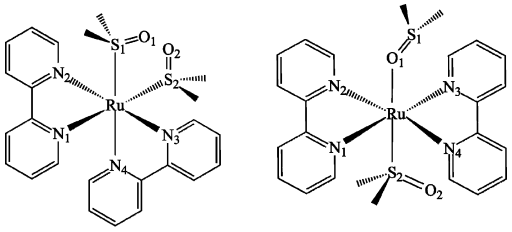

Scheme 2. Sequence of Reactions Experimentally Observed at Room Temperature after Photoexcitation for the cis (Left) and trans (Right) Isomers

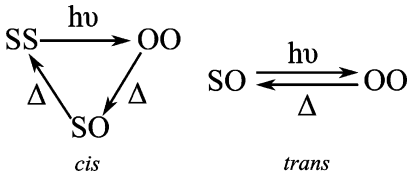

In this Article, we report a mechanistic study of the intramolecular S → O linkage photoisomerization in the *cis*- and *trans*-$[Ru(bpy)_2(DMSO)_2]^{2+}$ complexes. We identified an adiabatic isomerization path on the lowest triplet excited-state PES that allows the SS → OO isomerization of the cis isomer and the SO → OO isomerization of the trans isomer. We also localized some accessible deactivation funnels involved in nonadiabatic routes toward the GS in the vicinity of these paths. These data enabled us to compute the Gibbs activation energies of the adiabatic processes and the activation energies of the nonadiabatic processes and then, to establish a mechanistic picture of the linkage photoisomerization of the *cis*- and *trans*-$[Ru(bpy)_2(DMSO)_2]^{2+}$ complexes in DMSO. We propose two different accessible mechanisms for the cis isomer: a two-photon mechanism in which the absorption of each photon results in the linkage isomerization of one DMSO ligand, and a one-photon mechanism in which the absorption of one photon results in the sequential linkage isomerization of the two DMSO ligands. For the trans isomer, we propose a one-photon mechanism which results in its SO → OO linkage photoisomerization. We also show that the different topology of the triplet excited-state PES in the vicinity of the Franck−Condon region between the cis and trans isomers accounts for their different emission properties experimentally observed at low temperature.

2. COMPUTATIONAL DETAILS

For this study, Gaussian 09[49] (G09) and ORCA 2.9[50] codes were used to perform density functional theory (DFT) calculations. This theory has recently been applied to optimize triplet excited states of ruthenium polypyridine complexes and compare their relative energies in order to rationalize their photophysical properties.[51−59] In particular, DFT has been shown to describe reliably the relative energy of the relaxed ^{3}MLCT and ^{3}MC states versus ab initio methods.[60]

G09 was used for the gas phase optimization of all ground state and triplet excited state stationary points, and for their subsequent characterization as minimum or transition state (TS) using analytical harmonic vibrational frequency calculations. For these calculations, the MPWB1K[61] functional was used with two basis sets of increasing complexity: the simplest one denoted BS1 and the most extended one denoted BS2. BS2 is made of a Stuttgart relativistic small-core effective potential[62] for the ruthenium with its associated polarized basis set including two f and one g polarization functions,[63] a correlation-consistent polarized double-ζ basis set (cc-pVDZ)[64] for H atoms, and a correlation-consistent polarized triple-ζ basis set (cc-pVTZ)[64] for C, N, O, and S atoms. This calculation level (MPWB1K/BS2) was chosen for its reliability in computing the triplet potential energy landscape of the $[Ru(bpy)_2(OSO)]^+$ complex,[41,65] and for its accuracy in describing ground-state structures (see discussion in section 3.1). All calculations were performed without any symmetry constraints except for the GS structures *cis*-SS (C_2), *trans*-SS (C_i), and *trans*-OO (C_i). We also used G09 to perform gas phase intrinsic reaction coordinate[66] (IRC) calculations starting from the optimized triplet TS structures. This enabled us to identify the full isomerization reaction path on the triplet PES and to get detailed insight on the structural changes along this path. The MPWB1K functional was also used for IRC calculations but with a smaller basis set (BS1) because such calculations are very time-consuming. BS1 is composed of a double-ζ quality LANL2DZ[67] basis set for all atoms but the oxygen and the sulfur which were described by the 6-31G*[68] split valence Pople basis plus one polarization function. To compute the activation energies of the adiabatic processes in DMSO, we performed single point energy calculations at the ωB97XD[69]/BS2 computation level on the gas phase

dx.doi.org/10.1021/ic500546q | Inorg. Chem. 2014, 53, 6752−6760

optimized geometries and we used MPWB1K/BS2 to compute enthalpic and entropic corrections at 298 K. Tests using various functionals including dispersion terms or not were performed (Supporting Information Tables S1 and S2). The dispersion corrections stabilize the S-bonded coordination mode compared to the O-bonded one. In particular, with the ωB97XD functional, there is no ambiguity regarding the relative stability of the different cis isomers (the SS-bonded isomer being more stable than the SO-bonded isomer, the latter one being more stable than the OO-bonded isomer) in agreement with the experimental observations, whereas with MPWB1K, the energy differences in DMSO between the linkage isomers are rather small (especially between SS and SO isomers). We thus present energetic data computed with ωB97XD (note, however, that the triplet potential energy landscape obtained with MPWB1K and ωB97XD is very similar). We used the polarized continuum model[70] (PCM) as implemented in G09 to take solvent effects into account.

To find nonadiabatic routes along the photoisomerization pathway, we searched for minimum energy crossing points (MECPs) between the ground and lowest triplet states with Orca 2.9. Since MPWB1K is not available in the ORCA package, the calculation level PBE0-D3[71,72]/BS2 was used because it is in good agreement with experiment for the *cis*-SS structure. Triplet excited states and MECPs were thus optimized at this level, in the gas phase. Subsequently, activation energies in DMSO between a local minimum and the neighboring MECP were computed by performing single point energy calculations with the conductor like screening model (COSMO).[73]

The 0 → 0 emission energies from the SS-^{3}MLCT and OO-^{3}MLCT states for the cis isomer were obtained with G09 using the energy differences respectively with the SS-GS and OO-GS structures computed at the ωB97XD/BS2/PCM calculation level, including the zero point energy correction. Emission from the SS-^{3}MLCT state was computed in ethanol and emission from the OO-^{3}MLCT state was computed in DMSO to comply with the experimental conditions.[18]

In order to get insight in the electronic structure of the minima and of the TS, we used the canonical highest occupied molecular orbital (HOMO) and the canonical lowest unoccupied molecular orbital (LUMO) for the singlet closed shell structures and the singly occupied natural orbitals (SONOs) for the triplet structures. The SONOs are useful in case of open shell states to localize the unpaired electrons (two in triplet states) and thus, to quickly assess the MLCT or MC nature of a given excited state. In addition, the Mulliken spin density on the ruthenium atom is used to characterize the nature of the excited state: typically around 0.8 e^- for ^{3}MLCT states and 1.8 e^- for ^{3}MC states. For TS between ^{3}MLCT and ^{3}MC states, this spin density was found to be between 1.1 e^- and 1.3 e^-, showing the mixing of the two electronic states occurring at this geometry.

3. RESULTS AND DISCUSSION

3.1. Structures of the Ground State Minima. We optimized the three isomers SS, SO, and OO for *cis*- and *trans*-$[Ru(bpy)_2(DMSO)_2]^{2+}$ and their relevant geometrical parameters are reported in Table 1 (see Scheme 1 for atom labeling). The *trans*-SS isomer was not observed experimentally but our calculations show that this structure exists as a minimum on the ground state PES. The geometries in Cartesian coordinates and the canonical HOMO and LUMO of these minima are reported in Supporting Information Tables S3−S5 for the cis isomer and in Supporting Information Tables S6−S8 for the trans isomer. For each structure, the HOMO is a dπ metal centered orbital with some contributions of the ligands and the LUMO is a dπ* orbital localized on one or two bipyridine ligands. The deviations with respect to experiment[25] on the computed metal−ligand bond lengths are less than ∼0.01 Å for Ru−N bonds, and less than ∼0.03 Å for Ru−S bonds.

3.2. Ground State Isomerization Pathway. To characterize the thermal isomerization pathway, we investigated the ground state potential energy profiles (Table 2 and Supporting Information Figures S1 and S2). The optimization of the TS connecting the SS-GS and SO-GS minima (Supporting Information Tables S9 and S10) and the SO-GS and OO-GS minima (Supporting Information Tables S11 and S12) enables us to get the energetic data for all the stationary points in the ground electronic state. We can notice that the solvent (DMSO) has a dramatic effect since it strongly stabilizes the S-bonded coordination mode of the DMSO ligand compared to the O-bonded one. This is probably due to the fact that when a DMSO ligand is S-bonded, its terminal oxygen atom has a large solvent accessible surface. In the case of the cis isomer, taking the solvent into account changes the energy ordering obtained for the SS, SO and OO isomers and it is necessary to reproduce the relative stability SS > SO > OO observed experimentally in DMSO. For the trans isomer, both the results obtained in gas phase and in DMSO reproduce the relative stability observed experimentally with the SO minimum as the most stable one. From the kinetics point of view, for both cis and trans isomers, the transition states lie ca. 100 kJ mol^{-1} above the minimum, which means that thermal isomerization is not favorable.

Table 1. Computed Bond Lengths (Å) of the *cis*- and *trans*-SS, -SO, and -OO Isomers and Experimental Bond Lengths[25] in Parentheses

	cis			trans		
bond	SS (C_2)	SO	OO	SS (C_i)	SO	OO (C_i)
Ru−S_1	2.308 (2.281)			2.324		
Ru−S_2	2.308 (2.291)	2.270		2.324	2.232	
Ru−O_1		2.124	2.123		2.130	2.101
Ru−O_2			2.154			2.101
Ru−N_1	2.087 (2.093)	2.082	2.024	2.101	2.085	2.063
Ru−N_2	2.092 (2.097)	2.094	2.055	2.096	2.103	2.079
Ru−N_3	2.092 (2.086)	2.054	2.052	2.101	2.084	2.063
Ru−N_4	2.087 (2.099)	2.044	2.032	2.096	2.074	2.079

3.3. Exploration of the Lowest Triplet Excited-State Potential Energy Surfaces. To identify a reaction path which allows possible adiabatic *cis*-SS → *cis*-OO and *trans*-SO → *trans*-OO photoisomerizations, we explored the lowest triplet excited-state PESs. The geometry, the SONOs, and the Ru spin density of each stationary point involved along these paths are reported in Supporting Information Tables S13−S23 for the cis isomer and in Supporting Information Tables S24−S30 for the trans isomer. The gas phase energy profiles of the adiabatic reaction paths obtained from the IRC calculations are reported in Supporting Information Figures S3−S6 (cis isomer) and in Supporting Information Figures S7 and S8 (trans isomer). The electronic structure of the ^{3}MLCT states encountered along the isomerization path of the cis and trans isomers is described by a SONO localized on the ruthenium (dπ) and a SONO localized on one or two bipyridine ligands (dπ*). ^{3}MC states are described by the occupation of two metal-centered SONOs, a dπ orbital, and a dσ* orbital, which involves antibonding interactions between the metal and the ligands.

We will now describe the full adiabatic isomerization paths obtained for the cis (Figure 1) and the trans (Figure 2) isomers in terms of Gibbs energies in DMSO at 298 K. Gas phase energies, energies in DMSO and Gibbs energies in DMSO at 298 K are reported in Supporting Information Table S31 for the cis isomer and Supporting Information Table S32 for the trans isomer. The metal−ligand bond distances at the

dx.doi.org/10.1021/ic500546q | Inorg. Chem. 2014, 53, 6752−6760

Table 2. Computed Relative Gas Phase Energies, Energies in DMSO, and Gibbs Energies in DMSO at 298 K for the *cis*- and *trans*-SS, -SO, and -OO Isomers and Their Corresponding Transition States (kJ mol^{-1})

	cis			trans		
	ΔE_{gas}	ΔE_{DMSO}	ΔG_{DMSO}	ΔE_{gas}	ΔE_{DMSO}	ΔG_{DMSO}
SS	**0.0**	**0.0**	**0.0**	25.6	4.5	6.0
SS → SO TS	93.2	110.3	97.8	87.1	80.7	77.8
SO	−12.6	15.1	3.8	**0.0**	**0.0**	**0.0**
SO → OO TS	79.8	118.5	90.6	120.0	134.8	123.4
OO	−5.1	35.5	8.5	19.0	43.5	39.8

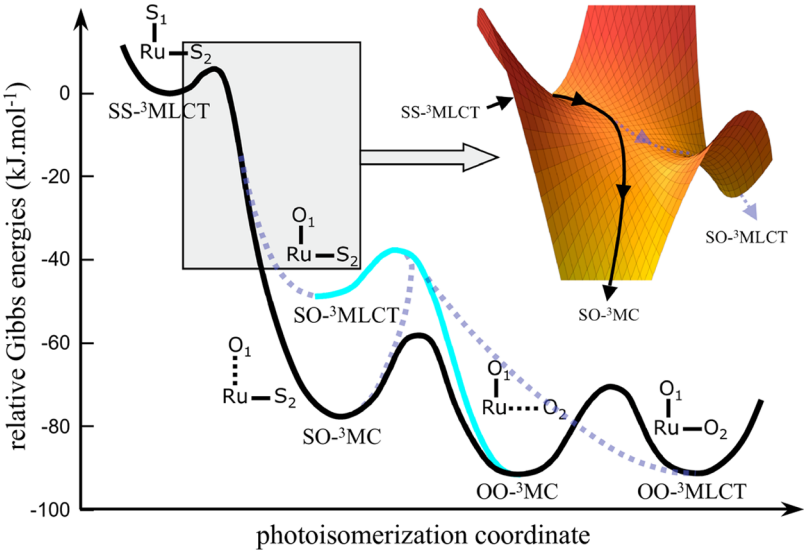

Figure 1. Gibbs energy profile in DMSO at 298 K of the adiabatic *cis*-SS → *cis*-OO photoisomerization paths. The Gibbs energies (Supporting Information Table S31) are arbitrarily given relative to the SS-^{3}MLCT state. The black line represents the lowest energy reaction path and the cyan line, an alternative path. Hypothetical higher energy pathways involving possible bifurcations are represented in dashed line. The inset schematically shows a possible bifurcation occurring after the first transition state encountered along the back path.

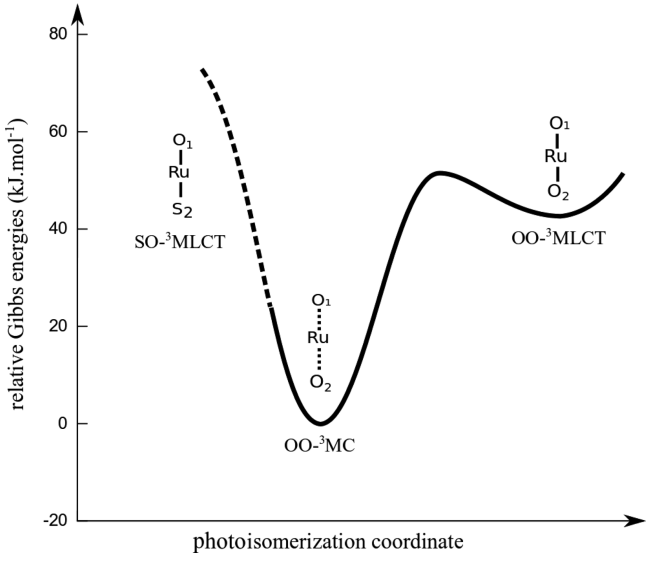

Figure 2. Gibbs energy profile in DMSO at 298 K of the adiabatic *trans*-SO → *trans*-OO photoisomerization path. The dashed line is based on the energetic data in DMSO (Supporting Information Table S32) and specifies that the Gibbs energy in DMSO is not available for the SO-^{3}MLCT structure since it is not a stationary point. The Gibbs energies are arbitrarily given relative to the OO-^{3}MC structure.

geometries of the minima are reported in Table 3 for the cis isomer and in Table 4 for the trans isomer.

Table 3. Metal−Ligand Distances (Å) in the Triplet Excited-State Minima Involved in the Adiabatic SS → OO Isomerization of the cis Isomer

bonds	SS-^{3}MLCT	SO-^{3}MC	SO-^{3}MLCT	OO-^{3}MC	OO-^{3}MLCT
Ru−S_1	2.377				
Ru−S_2	2.383	2.329	2.379		
Ru−O_1		2.525	2.062	2.089	2.033
Ru−O_2				2.601	2.082
Ru−N_1	2.083	2.091	2.049	2.366	1.995
Ru−N_2	2.116	2.089	2.100	2.120	2.027
Ru−N_3	1.982	2.142	2.032	2.055	2.075
Ru−N_4	2.041	2.377	1.980	2.067	2.036

Table 4. Metal−Ligand Distances (Å) in the Triplet Excited States Involved in the Adiabatic *trans*-SO → *trans*-OO Isomerization

bonds	OO-^{3}MC	OO-^{3}MLCT (C_1)
Ru−O_1	2.450	2.025
Ru−O_2	2.456	2.000
Ru−N_1	2.095	2.082
Ru−N_2	2.085	2.104
Ru−N_3	2.085	2.022
Ru−N_4	2.095	2.043

3.3.1. Adiabatic SS → OO Isomerization Path of cis-[Ru(bpy)$_2$(DMSO)$_2$]$^{2+}$. After photoexcitation to ^{1}MLCT states

dx.doi.org/10.1021/ic500546q | Inorg. Chem. 2014, 53, 6752−6760

(Supporting Information Figure S9), the commonly accepted relaxation scheme in polypyridyl ruthenium complexes involves ultrafast nonradiative processes from these initially populated states, which result eventually in the population of the lowest energy ^{3}MLCT excited state.[74] Optimization of this state (SS-^{3}MLCT) leads to the significant elongation (∼0.08 Å) of the two Ru−S bonds with respect to the SS-GS structure. This is in agreement with the substantial nuclear displacements observed in the ^{3}MLCT excited state after irradiation of another Ru(II) sulfoxide complex.[20] This shows that the Ru−S bond is weakened in the SS-^{3}MLCT state, which is favorable in view of the future linkage isomerization of the DMSO ligand. It should be noticed that the SS-^{3}MLCT structure has C_1 symmetry and that the promoted electron is localized on one single bipyridine ligand. This means that the C_2 symmetry of the SS-GS structure is broken during the relaxation of the Franck−Condon state toward the lowest triplet excited state. In the following, we discuss two possible scenarios for the relaxation from this SS-^{3}MLCT minimum: the first one describes the lowest energy pathway, which involves intermediates of ^{3}MC nature, the second one considers a pathway of ^{3}MLCT nature without intervention of ^{3}MC intermediates.

3.3.1.1. Lowest Energy Pathway Involving ^{3}MC States. The SS-^{3}MLCT state can relax to a SO-^{3}MC state (Supporting Information Figure S3), which is characterized by a strong distortion of the coordination sphere, as shown by the elongation of the Ru−N_4 bond in trans position to O_1 (Ru−O_1 = 2.525 Å, Ru−N_4 = 2.377 Å, Table 3). This geometry is usual for ^{3}MC states that are σ-antibonding along one single axis (N_4−Ru−O_1 in this case). The SS-^{3}MLCT → SO-^{3}MC step corresponds to the linkage isomerization of $DMSO_1$. The TS connecting the SS-^{3}MLCT and SO-^{3}MC minima is easily accessible from the SS-^{3}MLCT minimum since the corresponding Gibbs activation energy in DMSO is only 4.9 kJ mol^{-1} (Supporting Information Table S31). Its structure displays only little geometrical changes with respect to the SS-^{3}MLCT state, with an elongation of 0.131 Å for Ru−S_1 (Table 3). Note that the spin density on the ruthenium for this TS (1.17 e$^-$) has an intermediate value between the usual ones obtained for a ^{3}MLCT state (∼0.8 e$^-$) and a ^{3}MC state (∼1.8 e$^-$). This shows that the energy barrier of the SS-^{3}MLCT → SO-^{3}MC step is mainly associated with the changing nature of the electronic structure from ^{3}MLCT to ^{3}MC. At the TS, the SONO of the promoted electron involves significant contributions both from the ruthenium orbitals and from the bipyridine orbitals with the mixing of a metal-centered dσ*-like orbital and a bipyridine-centered π*-like orbital. The adiabatic linkage isomerization of the second S-bonded DMSO ($DMSO_2$) occurs from the SO-^{3}MC state to another ^{3}MC state (OO-^{3}MC, Supporting Information Figure S4).[75] This step combines four elementary events: (i) recoordination of the first isomerized DMSO ligand, (ii) shortening of the Ru−N_4 bond in trans position to $DMSO_1$ (Ru−O_1 = 2.089 Å, Ru−N_4 = 2.067 Å), (iii) decoordination and pirouetting of $DMSO_2$, and (iv) elongation of the Ru−N_1 bond in trans position to $DMSO_2$. The structure of the TS along the SO-^{3}MC → OO-^{3}MC step displays elongated metal−DMSO distances (Ru−S_2 = 2.629 Å, Ru−O_1 = 2.295 Å), which shows that the concomitant decoordination of the two DMSO ligands is required. The Gibbs activation energy along this step is relatively small ($\Delta G^{\ddagger}_{DMSO}$ = 19.2 kJ mol^{-1}). The last event of the adiabatic isomerization is the recoordination of $DMSO_2$ with a shortening of the Ru−O_2 bond from 2.601 to 2.082 Å together with the shortening of the Ru−N_1 bond in trans position from 2.366 to 1.995 Å, to populate the OO-^{3}MLCT state (Supporting Information Figure S5). The TS of the OO-^{3}MC → OO-^{3}MLCT step has an intermediate spin density value on the ruthenium (∼1.34 e$^-$), with the promoted electron localized both on the bipyridine and on the ruthenium. The Gibbs activation energy in DMSO along this step is $\Delta G^{\ddagger}_{DMSO}$ = 21.5 kJ mol^{-1}.

3.3.1.2. Higher Energy Pathway Involving ^{3}MLCT States. It is worth noting that a ^{3}MLCT minimum associated with a SO coordination scheme (SO-^{3}MLCT) with a lower energy than the SS-^{3}MLCT minimum was found. All our attempts to find a transition state directly connecting the SS-^{3}MLCT and the SO-^{3}MLCT minima failed. Three explanations can be put forward: (i) the transition state that connects the SS-^{3}MLCT and the SO-^{3}MC minima also connects the SS-^{3}MLCT and the SO-^{3}MLCT minima. This is possible if there is a post-transition transition state reaction pathway bifurcation[76] (as schematically drawn in inset of Figure 1). The nature of the transition vector (normal vibrational mode corresponding to the unique imaginary frequency) renders this hypothesis plausible, as this vibrational mode contains the right components to connect the SS-^{3}MLCT with both the SO-^{3}MC and SO-^{3}MLCT minima. Thus, the differentiation between the SS-^{3}MLCT → SO-^{3}MLCT and SS-^{3}MLCT → SO-^{3}MC pathways could occur after this transition state, or (ii) the transition state connecting the SS-^{3}MLCT and SO-^{3}MLCT minima lies at a higher energy than the one connecting the SS-^{3}MLCT and SO-^{3}MC minima, and the transition state search ends up finding the lowest transition state. In such a case, it would mean that the SS-^{3}MLCT → SO-^{3}MLCT pathway is kinetically less favorable, or (iii) there is in fact no transition state directly linking the SS-^{3}MLCT and SO-^{3}MLCT minima and the only possible route to access the SO-^{3}MLCT minimum on the lowest triplet potential energy surface is via the SO-^{3}MC state (SS-^{3}MLCT → SO-^{3}MC → SO-^{3}MLCT pathway).

Although we cannot definitely conclude on any of the three hypotheses above, a linearly interpolated transit path calculation between the SS-^{3}MLCT → SO-^{3}MC transition state and the SO-^{3}MLCT minimum (Supporting Information Figure S10) clearly shows that it is not possible to find an entire ^{3}MLCT pathway easily accessible. The linearly interpolated pathway displays a large potential energy barrier, which means that if a post-transition transition state reaction pathway bifurcation occurs (first hypothesis), this bifurcation must take place rather far away from the transition state. The linearly interpolated pathway also shows an excursion on the same triplet potential energy surface but with ^{3}MC character. Maintaining a ^{3}MLCT character throughout the S → O linkage isomerization would require imposing short Ru−S and Ru−O bond lengths in this system, which is somehow contradictory with the nuclear rearrangements required by the isomerization process. This would create a very large potential energy barrier. So, our conclusion is that, if there exists a SS-^{3}MLCT → SO-^{3}MLCT pathway, it will require an excursion on the triplet potential energy surface of ^{3}MC character.

Assuming that the SO-^{3}MLCT state can be populated, we could not identify an accessible pathway leading to the OO-^{3}MLCT minimum. For the same reasons mentioned above, no transition state directly linking the SO-^{3}MLCT minimum with the OO-^{3}MLCT minimum could be located. We believe that if there exists an SO-^{3}MLCT → OO-^{3}MLCT accessible pathway, it will also require an excursion on the

dx.doi.org/10.1021/ic500546q | Inorg. Chem. 2014, 53, 6752−6760

triplet potential energy surface of ^{3}MC character. Indeed, following the lowest energy pathway from the SO-^{3}MLCT state leads the system to relax in the OO-^{3}MC minimum (cyan path in Figure 1 and Supporting Information Figure S6) with the decoordination and linkage isomerization of the second S-bonded DMSO ligand (Ru−O_2 = 2.601 Å) together with the elongation of the Ru−N_1 bond in trans position from 2.049 to 2.366 Å. The Gibbs activation energy to overcome the transition state is small ($\Delta G^{\ddagger}_{DMSO}$ = 10.3 kJ mol^{-1}). Alternatively, the SO-^{3}MLCT state can relax back to the SO-^{3}MC minimum (dashed line in Figure 1) with the stretching of the Ru−O_1 distance (Ru−O_1 = 2.525 Å) following a higher energy pathway. Note that the same transition state is probably involved in both paths, as no other TS was located between the SO-^{3}MLCT and SO-^{3}MC minima.[77] Thus, another bifurcation is likely to occur after this transition state. In conclusion, a complete SS-^{3}MLCT → SO-^{3}MLCT → OO-^{3}MLCT pathway without intervention of ^{3}MC states is highly unlikely.

3.3.2. Adiabatic SO → OO Isomerization Path of trans-[Ru(bpy)$_2$(DMSO)$_2$]$^{2+}$. Similarly to the cis isomer, for the *trans*-SO isomer we assume that the lowest energy ^{3}MLCT excited state is populated after photoexcitation to ^{1}MLCT states (Supporting Information Figure S11) and subsequent relaxation from these states. Nevertheless, we did not find any stationary point on the triplet PES corresponding to a SO-bonded structure. Starting from the lowest triplet state at the SO-GS geometry, an IRC calculation, which follows the minimum energy path, leads to the inevitable linkage isomerization of $DMSO_2$ (Supporting Information Figure S7) and to the population of an OO-^{3}MC state where the two DMSO ligands are decoordinated (Ru−O > 2.45 Å, Table 4). It is worth noting that we found two minima corresponding to SS structures (SS-^{3}MLCT and SS-^{3}MC, Supporting Information Tables S24 and S26) with energies in DMSO lower than the SO-^{3}MLCT energy at the SO-GS geometry (Supporting Information Table S32). Thus, following excitation of SO-GS, both the SS structures and the OO-^{3}MC minimum may be populated, but the IRC calculation clearly shows that the S → O linkage isomerization of $DMSO_2$ is the most favorable relaxation path. The OO-^{3}MC state is connected to a OO-^{3}MLCT structure through a TS with a large Gibbs activation energy ($\Delta G^{\ddagger}_{DMSO}$ = 51.8 kJ mol^{-1}). Along the OO-^{3}MC → OO-^{3}MLCT step (Supporting Information Figure S8), the two Ru−O bonds shrink, ending at Ru−O_1 = 2.025 Å and Ru−O_2 = 2.000 Å.

3.3.3. Nonadiabatic Deactivation Processes. Since ^{3}MC states are known to deactivate nonradiatively toward the GS in ruthenium polypyridyl complexes, we were interested in finding accessible deactivation funnels along the triplet adiabatic isomerization paths previously described. We performed ground-state energy calculations along the triplet adiabatic isomerization paths obtained from the IRC calculations (Supporting Information Figures S12, S13). For the cis and trans isomers, the triplet-singlet energy difference becomes small in the region of ^{3}MC states. Thus, we searched for MECPs starting from ^{3}MC structures (*cis*-SO-^{3}MC, *cis*-OO-^{3}MC and *trans*-OO-^{3}MC). For each ^{3}MC minimum, a structurally similar MECP was found (Supporting Information Figures S14−S16). The main geometrical difference between the ^{3}MC state and its corresponding MECP is that the metal−ligand distances are even larger for the MECP.

The ^{3}MC → MECP activation energies in DMSO are respectively 20.0, 3.6, and 11.1 kJ mol^{-1} from the *cis*-SO-^{3}MC, *cis*-OO-^{3}MC and *trans*-OO-^{3}MC minima. Since these values are small, nonradiative deactivation toward the GS can be easily achieved from all three ^{3}MC minima.

3.4. Mechanisms for the SS → OO Photoisomerization of *cis*-[Ru(bpy)$_2$(DMSO)$_2$]$^{2+}$ and for the SO → OO Photoisomerization of *trans*-[Ru(bpy)$_2$(DMSO)$_2$]$^{2+}$. At this stage of our study, the computation of the adiabatic isomerization paths on the lowest triplet PES together with the localization of deactivation funnels toward the GS allow one to propose a mechanistic picture for the photoisomerization of the cis and trans isomers. The various photophysical processes (photoexcitation, adiabatic relaxation and intersystem crossing) and the minima involved in the isomerization mechanism, together with their connections, are reported in Figures 3 (cis isomer) and 4 (trans isomer). For clarity, the hypothetical higher energy reaction path *cis*-SS-^{3}MLCT → *cis*-SO-^{3}MLCT → *cis*-OO-^{3}MLCT (dashed line in Figure 1) is not displayed.

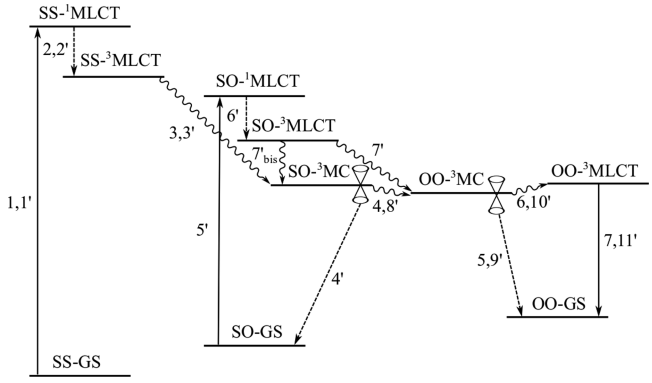

Figure 3. Schematic depiction of the major events involved in the stepwise *cis*-SS → *cis*-OO double photoisomerization mechanism. The various steps are labeled sequentially for the one-photon mechanism (1−7) and the two-photon mechanism (1′−11′). Solid arrows are used for absorption and emission, dashed arrows for intersystem crossings and curly arrows for adiabatic processes.

3.4.1. cis Isomer. We identified two different routes, which result in the population of the OO-^{3}MC state: one route where both DMSO ligands are isomerized sequentially with one photon (one-photon mechanism) and another one where one photon is required to isomerize each DMSO ligand (two-

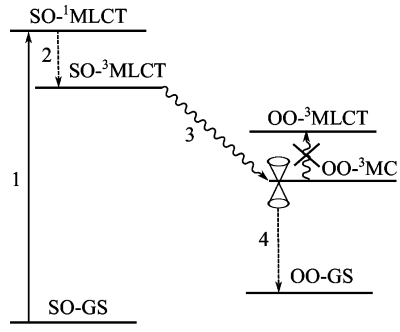

Figure 4. Schematic depiction of the SO → OO photoisomerization mechanism of the trans isomer. The various steps which result in the population of the OO-GS state are labeled sequentially (1−4) and their nature is specified using the same code as in Figure 3.

dx.doi.org/10.1021/ic500546q | Inorg. Chem. 2014, 53, 6752−6760

photon mechanism). The photoexcitation of the SS-GS structure leads to the population of the Franck−Condon state SS-^{1}MLCT (1, 1′). After relaxation to the lowest triplet excited state, the SS-^{3}MLCT minimum is populated (2, 2′) and the linkage isomerization of one DMSO ligand can take place to populate the SO-^{3}MC minimum (3, 3′). This minimum can be depopulated in two different ways, which give rise to the two different routes mentioned previously (one-photon mechanism and two-photon mechanism): (i) adiabatic relaxation toward the OO-^{3}MC state (4) ($\Delta E^{\ddagger}_{DMSO}$ = 18.5 kJ mol^{-1}, $\Delta G^{\ddagger}_{DMSO}$ = 19.2 kJ mol^{-1}), or (ii) nonradiative deactivation to SO-GS through intersystem crossing (4′) ($\Delta E^{\ddagger}_{DMSO}$ = 20.0 kJ mol^{-1}). On the basis of the magnitude of the activation energies, these two processes are equally favorable. However, other factors such as spin−orbit coupling (SOC) and nuclear reorganization will come into play to discriminate the mechanisms. Indeed, the population of the SO-GS minimum from the SO-^{3}MC state (4′) implies little structural changes but requires SOC, whereas the population of OO-^{3}MC requires large nuclear rearrangement but no SOC (4). Note that for the 4′ step, we cannot rule out that the SS-GS and OO-GS states be populated directly from the SO-^{3}MC state, but these deactivation pathways should be less favorable than 4′ since they would require major structural reorganizations. In the case that the SO-GS minimum is populated, a second photoexcitation is required to isomerize the second S-bonded DMSO ligand and can take place under the experimental conditions, since SO-GS and SS-GS absorb in the same region (λ_{max} = ∼410 and 348 nm, respectively).[18] Thus, the photoexcitation of the SO-GS state (5′) results in the population of the SO-^{3}MLCT minimum after relaxation of the SO-^{1}MLCT Franck−Condon state (6′). The SO-^{3}MLCT state can either adiabatically relax directly to the OO-^{3}MC minimum (7′) with the linkage isomerization of the second DMSO ligand or relax to this minimum in a two-step process via the SO-^{3}MC minimum ($7'_{bis}$, 8′). The same barrier of about 10 kJ mol^{-1} is involved in 7′ and $7'_{bis}$, thus both pathways are equally probable from a kinetic point of view. Finally, the depopulation of the OO-^{3}MC state can be achieved by two major processes: (i) nonadiabatic deactivation to OO-GS through intersystem crossing in the vicinity of the OO-^{3}MC state (5, 9′) ($\Delta E^{\ddagger}_{DMSO}$ = 3.6 kJ mol^{-1}) or (ii) adiabatic relaxation toward the OO-^{3}MLCT minimum (6, 10′) ($\Delta E^{\ddagger}_{DMSO}$ = 18.2 kJ mol^{-1}, $\Delta G^{\ddagger}_{DMSO}$ = 21.5 kJ mol^{-1}). Since ^{3}MLCT states are radiative in most ruthenium polypyridyl complexes, the population of the OO-^{3}MLCT state should lead to the emission of a photon (see section 3.5) and concomitant population of the OO-GS minimum (7, 11′).

3.4.2. trans Isomer. Photoexcitation of SO-GS (1) and subsequent relaxation of the Franck−Condon state (SO-^{1}MLCT) (2) result in the population of a SO-^{3}MLCT state. Since this state is not a minimum on the triplet PES, the adiabatic linkage isomerization of the S-bonded DMSO and the population of the OO-^{3}MC minimum occurs directly (3). Then, the OO-^{3}MC minimum can either nonadiabatically deactivate due to a nearby MECP ($\Delta E^{\ddagger}_{DMSO}$ = 11.1 kJ mol^{-1}) (4) or adiabatically form the OO-^{3}MLCT state ($\Delta E^{\ddagger}_{DMSO}$ = 35.9 kJ mol^{-1}, $\Delta G^{\ddagger}_{DMSO}$ = 51.8 kJ mol^{-1}). Since the energy barrier of the adiabatic process is much larger than the one computed for the nonadiabatic process, we expect the nonradiative deactivation of OO-^{3}MC to OO-GS to be largely favored. Deactivation of OO-^{3}MC to the SO-GS minimum (not shown on Figure 4) cannot be excluded.

3.5. Emission Properties. For the cis isomer, the 0 → 0 emission energy from the SS-^{3}MLCT state is predicted around 2.77 eV (448 nm), which is in good agreement with the experimental observation of 2.67 eV (465 nm) at 77 K. At low temperature in frozen medium, the population of the SO-^{3}MC state becomes less efficient and, consequently, the SS-^{3}MLCT state becomes emissive. This is consistent with the fact that at low temperature, the cis isomer displays no photochromism. Besides, the OO-^{3}MLCT state may be populated at room temperature during the photoisomerization of the cis isomer and in this case, the 0 → 0 emission energy is predicted around 1.620 eV (765 nm).

The trans isomer is nonemissive at room or low temperature. This is consistent with the fact that no SO-^{3}MLCT minimum was found on the triplet PES, and that the OO-^{3}MLCT state is hardly accessible after photoexcitation of *trans*-SO-GS. If the OO-^{3}MLCT state could nevertheless be populated, no emission would be anticipated due to the presence of the more stable and nonradiative OO-^{3}MC state. In addition, since the thermodynamics of the SO-^{3}MLCT → OO-^{3}MC step is so favorable, we believe that the trans isomer could display photochromism even at low temperature.

4. CONCLUSION

In this Article, we report a mechanistic study of the intramolecular S → O linkage photoisomerization of the *cis*- and *trans*-$[Ru(bpy)_2(DMSO)_2]^{2+}$ complexes. Reaction pathways that allow the adiabatic SS → OO isomerization of the cis isomer on the lowest triplet excited PES were identified. Along these paths, the S → O linkage isomerization of the two S-bonded DMSO ligands occurs sequentially following one-photon excitation of the SS isomer and is thermodynamically allowed throughout. As for the linkage photoisomerization of the bidentate OSO ligand in $[Ru(bpy)_2(OSO)]^+$,[42] following the population of the lowest ^{3}MLCT state that already elongates the Ru−S bond, the intervention of highly distorted ^{3}MC states is required to allow the large structural rearrangements occurring during the linkage isomerization of DMSO ligands.[41] A complete SS-^{3}MLCT → SO-^{3}MLCT → OO-^{3}MLCT pathway without intervention of ^{3}MC states is highly unlikely. In addition, some nonradiative deactivations toward the GS are favorable from ^{3}MC states, especially after the linkage isomerization of the first DMSO ligand. In this case, the SO-ground state is populated and a second photoexcitation is required to isomerize the second S-bonded DMSO ligand, which results in the proposed two-photon mechanism.

For the trans isomer, an adiabatic reaction pathway that allows the SO → OO isomerization on the lowest triplet PES was identified. Similarly to the cis isomer, a ^{3}MC state is involved along this path but nonradiative deactivation is predicted to occur predominantly after the linkage isomerization of the S-bonded DMSO ligand. It is noteworthy that, in this case, the isomerization on the triplet PES is a barrierless process. This peculiarity implies that the trans isomer has probably the same behavior at room temperature and at low temperature, namely the absence of emission from the SO-^{3}MLCT state and a photochromic behavior.

Finally, this study highlights the variety of processes that can be involved in the linkage photoisomerization of sulfoxide ligands in ruthenium polypyridyl complexes. The specificity of the topology of the triplet PES together with the coexistence of adiabatic and nonadiabatic processes in these complexes are responsible for their rich photophysical and photochemical

dx.doi.org/10.1021/ic500546q | Inorg. Chem. 2014, 53, 6752−6760

properties. Furthermore, this study confirms that DFT calculations can be an efficient tool to investigate excited state events involved in the linkage photoisomerization of ambidentate ligands in transition metal complexes. Our next goal will be to investigate the photoisomerization mechanism of osmium sulfoxide complexes for which MC states are expected to be too high in energy to play any role in this mechanism. In these complexes, we expect the photoisomerization mechanism to only involve the lowest MLCT excited state.

■ ASSOCIATED CONTENT

Supporting Information

Tables S1−S2 for test calculations using different functionals, Tables S3−S30 for Cartesian coordinates, energies, and orbitals of all the optimized stationary points, Tables S31−S32 for relative energies along the adiabatic photoisomerization pathways, Figures S1−S2 for thermal isomerization energy profiles, Figures S3−S8 for IRC calculations, Figures S9 and S11 for computed absorption spectra, Figure S10 for linearly interpolated transit path calculation, Figures S12−S13 for singlet−triplet energy difference along the adiabatic photoisomerization pathways, and Figures S14−S16 for structures of MECPs. This material is available free of charge via the Internet at http://pubs.acs.org.

■ AUTHOR INFORMATION

Corresponding Author

*E-mail: martial.boggio@irsamc.ups-tlse.fr.

Notes

The authors declare no competing financial interest.

■ ACKNOWLEDGMENTS

This work was granted access to the HPC resources of CALMIP under the allocation 2013-[0880]. The authors thank Professor Jeffrey J. Rack for his interest in this work and valuable discussions helping to improve this manuscript.

■ REFERENCES

(1) Straight, S. D.; Andreasson, J.; Kodis, G.; Bandyopadhyay, S.; Mitchell, R. H.; Moore, T. A.; Moore, A. L.; Gust, D. *J. Am. Chem. Soc.* **2005**, *127*, 9403−9409.

(2) Straight, S. D.; Andreasson, J.; Kodis, G.; Moore, A. L.; Moore, T. A.; Gust, D. *J. Am. Chem. Soc.* **2005**, *127*, 2717−2724.

(3) Bonnet, S.; Collin, J.-P.; Sauvage, J.-P. *Inorg. Chem.* **2006**, *45*, 4024−4034.

(4) Yu, Y. L.; Nakano, M.; Ikeda, T. *Nature* **2003**, *425*, 145−145.

(5) Schaefer, L. V.; Mueller, E. M.; Gaub, H. E.; Grubmueller, H. *Angew. Chem., Int. Ed.* **2007**, *46*, 2232−2237.

(6) Eelkema, R.; Pollard, M. M.; Vicario, J.; Katsonis, N.; Ramon, B. S.; Bastiaansen, C. W. M.; Broer, D. J.; Feringa, B. L. *Nature* **2006**, *440*, 163.

(7) Natansohn, A.; Rochon, P. *Chem. Rev.* **2002**, *102*, 4139−4175.

(8) Hugel, T.; Holland, N. B.; Cattani, A.; Moroder, L.; Seitz, M.; Gaub, H. E. *Science* **2002**, *296*, 1103−1106.

(9) Al-Atar, U.; Fernandes, R.; Johnsen, B.; Baillie, D.; Branda, N. R. *J. Am. Chem. Soc.* **2009**, *131*, 15966−15967.

(10) Gorostiza, P.; Isacoff, E. Y. *Science* **2008**, *322*, 395−399.

(11) Guetlich, P.; Garcia, Y.; Woike, T. *Coord. Chem. Rev.* **2001**, *219*, 839−879.

(12) Coppens, P.; Novozhilova, I.; Kovalevsky, A. *Chem. Rev.* **2002**, *102*, 861−883.

(13) Bitterwolf, T. E. *Coord. Chem. Rev.* **2006**, *250*, 1196−1207.

(14) To, T. T.; Heilweil, E. J.; Duke, C. B.; Ruddick, K. R.; Webster, C. E.; Burkey, T. J. *J. Phys. Chem. A* **2009**, *113*, 2666−2676.

(15) Johnson, D. A.; Dew, V. C. *Inorg. Chem.* **1979**, *18*, 3273−3274.

(16) Sylvester, S. O.; Cole, J. M.; Waddell, P. G. *J. Am. Chem. Soc.* **2012**, *134*, 11860−11863.

(17) Rack, J. J.; Winkler, J. R.; Gray, H. B. *J. Am. Chem. Soc.* **2001**, *123*, 2432−2433.

(18) Rack, J. J.; Mockus, N. V. *Inorg. Chem.* **2003**, *42*, 5792−5794.

(19) Lutterman, D. A.; Rachford, A. A.; Rack, J. J.; Turro, C. *J. Phys. Chem. Lett.* **2010**, *1*, 3371−3375.

(20) McClure, B. A.; Abrams, E. R.; Rack, J. J. *J. Am. Chem. Soc.* **2010**, *132*, 5428−5436.

(21) McClure, B. A.; Rack, J. J. *Inorg. Chem.* **2011**, *50*, 7586−7590.

(22) Porter, B. L.; McClure, B. A.; Abrams, E. R.; Engle, J. T.; Ziegler, C. J.; Rack, J. J. *J. Photochem. Photobiol. A: Chem.* **2011**, *217*, 341−346.

(23) Jin, Y.; Rack, J. J. *Isr. J. Chem.* **2013**, *53*, 280−287.

(24) King, A. W.; Jin, Y.; Engle, J. T.; Ziegler, C. J.; Rack, J. J. *Inorg. Chem.* **2013**, *52*, 2086−2093.

(25) Smith, M. K.; Gibson, J. A.; Young, C. G.; Broomhead, J. A.; Junk, P. C.; Keene, F. R. *Eur. J. Inorg. Chem.* **2000**, *6*, 1365−1370.

(26) Rack, J. J. *Coord. Chem. Rev.* **2009**, *253*, 78−85 and references therein..

(27) McClure, B. A.; Rack, J. J. *Eur. J. Inorg. Chem.* **2010**, *25*, 3895−3904.

(28) (a) Celani, P.; Bernardi, F.; Olivucci, M.; Robb, M. A. *J. Am. Chem. Soc.* **1997**, *119*, 10815−10820. (b) Boggio-Pasqua, M.; Bearpark, M. J.; Hunt, P. A.; Robb, M. A. *J. Am. Chem. Soc.* **2002**, *124*, 1456−1470. (c) Boggio-Pasqua, M.; Ravaglia, M.; Bearpark, M. J.; Garavelli, M.; Robb, M. A. *J. Phys. Chem. A* **2003**, *107*, 11139−11152. (d) Gomez, I.; Reguero, M.; Robb, M. A. *J. Phys. Chem. A* **2006**, *110*, 3986−3991. (e) Boggio-Pasqua, M.; Bearpark, M. J.; Robb, M. A. *J. Org. Chem.* **2007**, *72*, 4497−4503. (f) Tomasello, G.; Ogliaro, F.; Bearpark, M. J.; Robb, M. A.; Garavelli, M. *J. Phys. Chem. A* **2008**, *112*, 10096−10107. (g) Tomasello, G.; Bearpark, M. J.; Robb, M. A.; Orlandi, G.; Garavelli, M. *Angew. Chem., Int. Ed.* **2010**, *49*, 2913−2916.

(29) (a) Zgierski, M. Z.; Grabowska, A. *J. Chem. Phys.* **2000**, *112*, 6329−6337. (b) Zgierski, M. Z.; Grabowska, A. *J. Chem. Phys.* **2000**, *113*, 7845−7852.

(30) Migani, A.; Gentili, P. L.; Negri, F.; Olivucci, M.; Romani, A.; Favaro, G.; Becker, R. S. *J. Phys. Chem. A* **2005**, *109*, 8684−8692.

(31) Ortiz-Sánchez, J. M.; Gelabert, R.; Moreno, M.; Lluch, J. M. *J. Phys. Chem. A* **2006**, *110*, 4649−4656.

(32) Maurel, F.; Aubard, J.; Millie, P.; Dognon, J. P.; Rajzmann, M.; Guglielmetti, R.; Samat, A. *J. Phys. Chem. A* **2006**, *110*, 4759−4771.

(33) Nakamura, S.; Yokojima, S.; Uchida, K.; Tsujioka, T.; Goldberg, A.; Murakami, A.; Shinoda, K.; Mikami, M.; Kobayashi, T.; Kobatake, S.; Matsuda, K.; Irie, M. *J. Photochem. Photobiol. A: Chem.* **2008**, *200*, 10−18.

(34) Mikhailov, I. A.; Belfield, K. D.; Masunov, A. E. *J. Phys. Chem. A* **2009**, *113*, 7080−7089.

(35) Sanchez-Lozano, M.; Estevez, C. M.; Hermida-Ramon, J.; Serrano-Andres, L. *J. Phys. Chem. A* **2011**, *115*, 9128−9138.

(36) Nenov, A.; Schreier, W. J.; Koller, F. O.; Braun, M.; de Vivie-Riedle, R.; Zinth, W.; Pugliesi, I. *J. Phys. Chem. A* **2012**, *116*, 10518−10528.

(37) Raymo, F. M. *J. Phys. Chem. A* **2012**, *116*, 11888−11895.

(38) Schoenborn, J. B.; Hartke, B. *J. Photochem. Photobiol. A: Chem.* **2013**, *263*, 34−40.

(39) Liu, F.; Morokuma, K. *J. Am. Chem. Soc.* **2013**, *135*, 10693−10702.

(40) Ciofini, I.; Daul, C. A.; Adamo, C. *J. Phys. Chem. A* **2003**, *107*, 11182−11190.

(41) Goettle, A. J.; Dixon, I. M.; Alary, F.; Heully, J.-L.; Boggio-Pasqua, M. *J. Am. Chem. Soc.* **2011**, *133*, 9172−9174.

(42) McClure, B. A.; Mockus, N. V.; Butcher, D. P.; Lutterman, D. A.; Turro, C.; Petersen, J. L.; Rack, J. J. *Inorg. Chem.* **2009**, *48*, 8084−8091.

(43) Rachford, A. A.; Petersen, J. L.; Rack, J. J. *Inorg. Chem.* **2005**, *44*, 8065−8075.

(44) Rachford, A. A.; Petersen, J. L.; Rack, J. J. *Inorg. Chem.* **2006**, *45*, 5953−5960.

(45) Mockus, N. V.; Petersen, J. L.; Rack, J. J. *Inorg. Chem.* **2006**, *45*, 8−10.
(46) Lutterman, D. A.; Rachford, A. A.; Rack, J. J.; Turro, C. *J. Phys. Chem. A* **2009**, *113*, 11002−11006.
(47) Garg, K.; Engle, J. T.; Ziegler, C. J.; Rack, J. J. *Chem.—Eur. J.* **2013**, *19*, 11686−11695.
(48) Garg, K.; King, A. W.; Rack, J. J. *J. Am. Chem. Soc.* **2014**, *136*, 1856−1863.
(49) Frisch, M. J.; Trucks, G. W.; Schlegel, H. B.; Scuseria, G. E.; Robb, M. A.; Cheeseman, J. R.; Scalmani, G.; Barone, V.; Mennucci, B.; Petersson, G. A.; Nakatsuji, H.; Caricato, M.; Li, X.; Hratchian, H. P.; Izmaylov, A. F.; Bloino, J.; Zheng, G.; Sonnenberg, J. L.; Hada, M.; Ehara, M.; Toyota, K.; Fukuda, R.; Hasegawa, J.; Ishida, M.; Nakajima, T.; Honda, Y.; Kitao, O.; Nakai, H.; Vreven, T.; Montgomery, Jr., J. A.; Peralta, J. E.; Ogliaro, F.; Bearpark, M.; Heyd, J. J.; Brothers, E.; Kudin, K. N.; Staroverov, V. N.; Kobayashi, R.; Normand, J.; Raghavachari, K.; Rendell, A.; Burant, J. C.; Iyengar, S. S.; Tomasi, J.; Cossi, M.; Rega, N.; Millam, J. M.; Klene, M.; Knox, J. E.; Cross, J. B.; Bakken, V.; Adamo, C.; Jaramillo, J.; Gomperts, R.; Stratmann, R. E.; Yazyev, O.; Austin, A. J.; Cammi, R.; Pomelli, C.; Ochterski, J. W.; Martin, R. L.; Morokuma, K.; Zakrzewski, V. G.; Voth, G. A.; Salvador, P.; Dannenberg, J. J.; Dapprich, S.; Daniels, A. D.; Farkas, Ö.; Foresman, J. B.; Ortiz, J. V.; Cioslowski, J.; Fox, D. J. *Gaussian 09*, revision A.2; Gaussian, Inc., Wallingford CT, 2009.
(50) Neese, F. *ORCA—An Ab Initio, DFT and Semiempirical Program Package*, version 2.9; University of Bonn: Bonn, Germany, 2012.
(51) Alary, F.; Heully, J.-L.; Bijeire, L.; Vicendo, P. *Inorg. Chem.* **2007**, *46*, 3154−3165.
(52) Alary, F.; Boggio-Pasqua, M.; Heully, J.-L.; Marsden, C. J.; Vicendo, P. *Inorg. Chem.* **2008**, *47*, 5259−5266.
(53) Heully, J.-L.; Alary, F.; Boggio-Pasqua, M. *J. Chem. Phys.* **2009**, *131*, 184308.
(54) Lebon, E.; Bastin, S.; Sutra, P.; Vendier, L.; Piau, R. E.; Dixon, I. M.; Boggio-Pasqua, M.; Alary, F.; Heully, J.-L.; Igau, A.; Juris, A. *Chem. Commun.* **2012**, *48*, 741−743.
(55) Piau, R. E.; Guillon, T.; Lebon, E.; Perrot, N.; Alary, F.; Boggio-Pasqua, M.; Heully, J.-L.; Juris, A.; Sutra, P.; Igau, A. *New J. Chem.* **2012**, *36*, 2484−2492.
(56) Österman, T.; Abrahamsson, M.; Becker, H.-C.; Hammarström, L.; Persson, P. *J. Phys. Chem. A* **2012**, *116*, 1041−1050.
(57) Vallett, P. J.; Damrauer, N. H. *J. Phys. Chem. A* **2013**, *117*, 6489−6507.
(58) Garino, C.; Salassa, L. *Philos. Trans. R. Soc. A* **2013**, *371*, 20120134.
(59) Lebon, E.; Sylvain, R.; Piau, R. E.; Lanthony, C.; Pilmé, J.; Sutra, P.; Boggio-Pasqua, M.; Heully, J.-L.; Alary, F.; Juris, A.; Igau, A. *Inorg. Chem.* **2014**, *53*, 1946−1948.
(60) Guillon, T.; Boggio-Pasqua, M.; Alary, F.; Heully, J.-L.; Lebon, E.; Sutra, P.; Igau, A. *Inorg. Chem.* **2010**, *49*, 8862−8872.
(61) Zhao, Y.; Truhlar, D. G. *J. Phys. Chem. A* **2004**, *108*, 6908−6918.
(62) Andrae, D.; Haussermann, U.; Dolg, M.; Stoll, H.; Preuss, H. *Theor. Chim. Acta* **1990**, *77*, 123−141.
(63) Martin, J. M. L.; Sundermann, A. *J. Chem. Phys.* **2001**, *114*, 3408−3420.
(64) Dunning, T. H. *J. Chem. Phys.* **1989**, *90*, 1007−1023.
(65) Göttle, A. J. Etude théorique de propriétés photophysiques et photochimiques de complexes de ruthenium. Ph.D. Dissertation, Université Toulouse 3 Paul Sabatier, 2013. Downloadable on DART-Europe E-theses Portal (www.dart-europe.eu).
(66) (a) Hratchian, H. P.; Schlegel, H. B. *J. Chem. Phys.* **2004**, *120*, 9918−9924. (b) Hratchian, H. P.; Schlegel, H. B. In *Theory and Applications of Computational Chemistry: The First Forty Years*; Dykstra, C. E., Frenking, G., Kim, K. S., Scuseria, G. E., Eds.; Elsevier: Amsterdam, 2005; pp 195−249.
(67) (a) Dunning, Jr., T. H.; Hay, P. J. In *Modern Theoretical Chemistry*; Schaefer, III, H. F., Ed.; Plenum: New York, 1976; pp 1−28. (b) Hay, P. J.; Wadt, W. R. *J. Chem. Phys.* **1985**, *82*, 299−310.
(68) (a) Hehre, W. J.; Ditchfield, R.; Pople, J. A. *J. Chem. Phys.* **1972**, *56*, 2257−2261. (b) Hariharan, P. C.; Pople, J. A. *Theor. Chim. Acta* **1973**, *28*, 213−222. (c) Francl, M. M.; Pietro, W. J.; Hehre, W. J.; Binkley, J. S.; Gordon, M. S.; DeFrees, D. J.; Pople, J. A. *J. Chem. Phys.* **1982**, *77*, 3654−3665.
(69) Chai, J.-D.; Head-Gordon, M. *Phys. Chem. Chem. Phys.* **2008**, *10*, 6615−6620.
(70) (a) Tomasi, J.; Mennucci, B.; Cammi, R. *Chem. Rev.* **2005**, *105*, 2999−3093. (b) Scalmani, G.; Frisch, M. J. *J. Chem. Phys.* **2010**, *132*, No. 114110.
(71) Adamo, C.; Barone, V. *J. Chem. Phys.* **1999**, *110*, 6158−6170.
(72) Grimme, S.; Antony, J.; Ehrlich, S.; Krieg, H. *J. Chem. Phys.* **2010**, *132*, No. 154104.
(73) Klamt, A. *J. Phys. Chem.* **1995**, *99*, 2224−2235.
(74) Damrauer, N. H.; Cerullo, G.; Yeh, A.; Boussie, T. R.; Shank, C. V.; McCusker, J. K. *Science* **1997**, *275*, 54−57.
(75) Another minimum of ^{3}MC nature with two O-bonded DMSO ligands (OO-^{3}MC′, Supporting Information Table S19) was found on the isomerization path but it has a very similar geometry and it is almost degenerate with OO-^{3}MC, so we did not report it in the discussion for clarity.
(76) Ess, D. H.; Wheeler, S. E.; Iafe, R. G.; Xu, L.; Celebi-Olçüm, N.; Houk, K. N. *Angew. Chem., Int. Ed.* **2008**, *47*, 7592−7601.
(77) A TS search between the SO-^{3}MLCT and SO-^{3}MC minima leads to the SO-^{3}MLCT/OO-^{3}MC TS.